Arch. Metall. Mater. **69** (2024), 1, 129-133

DOI: https://doi.org/10.24425/amm.2024.147800

JIN KWANG JANG[1], JAEYUN MOON[2], JONGMIN BYUN[1,3*]

SYNTHESIS OF POLYCRYSTALLINE BI-DOPED SNSE BY MECHANICAL ALLOYING AND HYDROGEN REDUCTION

In this study, Bi-doped SnSe was fabricated through the high energy ball milling and the hydrogen reduction of Bi_2O_3, and its thermoelectric properties were analyzed. The specimen with pure-Bi was fabricated as a control group and properties were compared. In the case of specimens with added Bi_2O_3, when sintering was performed in a hydrogen atmosphere, Bi_2O_3 with a high melting point was reduced to Bi with a relatively low melting point. At this time, because of the appearance of the liquid phase, the orientation of the (400) plane increased, and the density was improved. As a result, the change of SnSe to n-type was confirmed in the temperature range of 300 K - 773 K due to Bi doping. Additionally, when Bi_2O_3 was used instead of pure-Bi, the thermal conductivity, which is inversely proportional to the figure of merit, decreased, and the electrical conductivity increased, resulting in an improvement in the figure of merit.

Keywords: SnSe; Thermoelectric properties; Hydrogen reduction; N-type; Bi_2O_3

1. Introduction

Today, interest in energy recycling is continuously increasing due to the problems of resource depletion and environmental pollution. In accordance with this interest, interest in energy harvesting, which recycles waste energy such as pressure, light energy, electromagnetic waves, and waste heat, is increasing. Among them, there is increasing interest in thermoelectric materials that can convert waste heat generated from factories, transportation, and the body into electrical energy by using the Seebeck effect [1].

Generally, thermoelectric materials exhibit varying performances dependent on their chemical composition and operating temperature, and their performance is quantified by the figure of merit (ZT). The figure of merit is expressed by the equation, $ZT = \frac{S^2\sigma}{\kappa}T$, where S is the Seebeck coefficient, σ is the electrical conductivity, and κ is the total thermal conductivity. As the equation suggests, to increase the figure of merit ZT, the power factor must be increased, and the total thermal conductivity must be reduced [2].

Thermoelectric materials are divided into low-temperature, medium-temperature, and high-temperature thermoelectric materials according to their maximum efficiency temperature. Many studies are being conducted to improve thermoelectric performance by using Bi_2Te_3 [3,4] in the low-temperature region, PbTe [5] and Se-based compound [6,7] in the medium-temperature region. In the high-temperature region, oxides like BiCuSeO [8] are actively studied. Among these materials, tin selenide (SnSe) does not contain any toxic element such as Pb, has the advantage of being composed of elements abundant on earth and has its own low thermal conductivity due to the anisotropy and inharmonic structure resulting from the layered structure. For these reasons, a lot of research is being conducted on SnSe, which shows a high figure of merit in the medium temperature region [9].

Since SnSe inherently has p-type characteristics, many studies on p-type have been conducted, but both n-type and p-type are needed to fabricate devices [10]. Accordingly, research was conducted to change the type of SnSe with good thermoelectric properties. The method of doping other elements for type change was used, and a high figure of merit was reported by doping Bi into single crystal SnSe [11]. In the case of single-crystal SnSe, due to the complex process and weak mechanical properties, many studies have been conducted to try to change the type by doping Bi into polycrystalline SnSe [12-14]. Recent studies on SnSe have extensively utilized ball milling for SnSe synthesis.

[1] SEOUL NATIONAL UNIVERSITY OF SCIENCE AND TECHNOLOGY, DEPARTMENT OF MATERIALS SCIENCE AND ENGINEERING, SEOUL 01811, REPUBLIC OF KOREA
[2] UNIVERSITY OF NEVADA, LAS VEGAS, DEPARTMENT OF MECHANICAL ENGINEERING, 4505 S. MARYLAND PKWY LAS VEGAS, NV 89154, UNITED STATES
[3] SEOUL NATIONAL UNIVERSITY OF SCIENCE AND TECHNOLOGY, THE INSTITUTE OF POWDER TECHNOLOGY, SEOUL 01811, REPUBLIC OF KOREA

* Corresponding author: byun@seoultech.ac.kr

Additionally, pressure sintering has been used to effectively suppress grain growth. However, pressure sintering has limitations in terms of initial powder selection due to difficulties in controlling the atmosphere.

Therefore, in this study, $Sn_{0.94}Bi_{0.06}Se$ was fabricated by high energy ball milling and pressureless sintering in a hydrogen atmosphere using Sn, Se, and Bi_2O_3 as starting powders, and its thermoelectric properties were measured at 300 K - 773 K. For the control group, the same experiment was conducted using pure-Bi instead of Bi_2O_3. When Bi2O3 was used, we observed an increase in the figure of merit. This enhancement was attributed to increased density and the improved orientation of the a-axis plane, which resulted from the formation of a liquid phase during the reduction of Bi_2O_3 to Bi.

2. Experimental

Sn (~45 μm, 99.9%, Avention), Se (~45 μm, 99.9%, Avention), Bi (~30 μm, 99.9%, Avention), and Bi_2O_3 (~100 nm, 99.9%, Avention) were used in this experiment. They were weighted to satisfy the composition of $Sn_{0.94}Bi_{0.06}Se$. High energy ball milling was performed for 50 h at a speed of 250 rpm using a planetary ball mill (Retsch, PM 400) in milling jar (STD 11). High-energy ball milling was performed in Ar atmosphere to avoid oxidation by air. The ratio of stainless steel (STS 304) balls with a diameter of 4.76 mm to the powder was 10:1 (wt.%). Process control agent (PCA) was not added to prevent oxidation. To minimize the effect of the heat generated by collision between the stainless steel ball and the milling jar, the experiment was conducted with a running time of 20 min and a break time of 10 min. For the classification of specimens, powders and specimens made using Sn, Se, and Bi_2O_3 are referred to as Bi_2O_3-$Sn_{0.94}Bi_{0.06}Se$, while powders and specimens made using Sn, Se, and Bi are referred to as Bi-$Sn_{0.94}Bi_{0.06}Se$.

To prepare the green body, 0.8 g of powder was maintained at about 500 MPa for 1 min using a die with a diameter of 10 mm and a uniaxial compaction. For sintering, a tube furnace was used, and the atmosphere was maintained for 10 min at a flow rate of 0.7 L/min using Ar gas to avoid reaction with elements in the air. Then, the temperature was raised to 550°C at a heating rate of 10°C/min. After that, pressureless sintering was performed for 2 h at a flow rate of 0.8 L/min in H_2 atmosphere, followed by furnace cooling. X-Ray diffractometer (XRD) (Rigaku, Miniflex 300) was used for phase analysis of the specimens, and Particle Size Analysis (PSA) was also performed to analyze the particle size. Microstructure observation and Energy Dispersive X-ray Spectroscopy (EDS) mapping were performed using Scanning Electron Microscopy (SEM, Hitachi High-tech, U8010). Electrical conductivity and Seebeck coefficient were measured in a direction parallel to the compaction direction at room temperature and at the temperature ranging from 323 K to 773 K using ZEM-3 (Ulvac, M8). Thermal conductivity was measured in a direction parallel to the compaction direction at the same temperature as the temperature at which the electrical conductivity and Seebeck coefficient were measured using Laser Flash Analysis (NETZSCH, LFA-457HT).

3. Results and discussion

Fig. 1 shows the XRD patterns of the ball-milled powder and sintered body. In Fig. 1(a), the peak of the XRD pattern corresponding to powder containing pure Bi was shifted toward a smaller angle. Considering the Bragg diffraction law ($n\lambda = 2d\sin\theta$), it can be expected that when an atom with a large atomic radius replaces an atom with a small atomic radius, the interplanar distance widens and the peak moves to the smaller side [15]. Bi (1.63 Å), which has a relatively large atomic radius, replaced the position of Sn (1.22 Å) [14], which has a relatively small atomic radius. Hence, the interplanar distance widened and the peak shifted to the smaller side. In Fig. 1(b), it can be confirmed that Bi_2O_3 is reduced under the influence of sintering in a hydrogen atmosphere to form a Bi peak. In the patterns

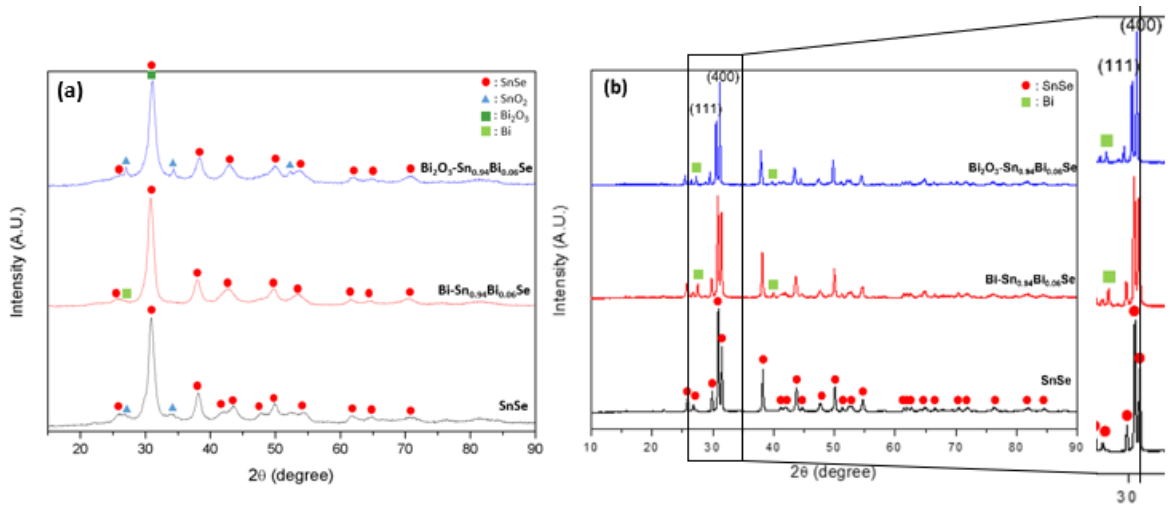

Fig. 1. XRD patterns of (a) ball-milled powder, and (b) sintered body. The black line is for the experiment with Sn and Se. The red line is for the experiment with Bi, Sn, and Se. And the blue line is for the experiment with Bi_2O_3, Sn, and Se

of SnSe and Bi-$Sn_{0.94}Bi_{0.06}Se$, the intensity of the (111) plane peak was higher than that of the (400) plane peak. However, in the pattern of Bi_2O_3-$Sn_{0.94}Bi_{0.06}Se$, the intensity of the (400) plane peak was higher than that of the (111) plane peak. This phenomenon occurred due to the appearance of a liquid phase during the process of reducing Bi_2O_3, which has a high melting point (817°C), to Bi, which has a low melting point (271°C) [16]. It is observed that the (111) peak of the pattern of SnSe was 31.72°, while the (111) peaks of the pattern of Bi-$Sn_{0.94}Bi_{0.06}Se$ and Bi_2O_3-$Sn_{0.94}Bi_{0.06}Se$ were 31.66° and 31.46°, respectively. This is thought to be the result of Bi replacing the position of Sn.

Fig. 2 shows milled powder SEM images. The SEM image of the powder in Fig. 2 shows no significant difference in powder shape, but it was confirmed that the particle size of the powder milled using Bi was small, and PSA analysis was performed for more quantitative analysis. Based on the PSA analysis (TABLE 1), the particle size of the powder milled with Bi was d_{50}: 2.431 µm, while those of the powder milled with Sn and Se and the powder milled with Bi_2O_3, Sn, and Se were d_{50}: 3.461 µm and d_{50}: 3.878 µm, respectively. The brittleness of the combined powder increased upon the addition of Bi, which is widely recognized for its brittleness. Therefore, the milling impact was enhanced, as a result, milled Bi-$Sn_{0.94}Bi_{0.06}Se$ particles became fine powders [17,18].

TABLE 1

PSA results of ball-milled SnSe, Bi-$Sn_{0.94}Bi_{0.06}Se$, and Bi_2O_3-$Sn_{0.94}Bi_{0.06}Se$ powder

	SnSe	**Bi-$Sn_{0.94}Bi_{0.06}Se$**	**Bi_2O_3-$Sn_{0.94}Bi_{0.06}Se$**
d_{10} (µm)	0.79	0.83	1.04
d_{50} (µm)	3.46	2.43	3.88
d_{90} (µm)	12.28	9.54	15.8
d_{100} (µm)	43.67	36.24	52.62

SEM images and EDS mapping of the sintered body are shown in Fig. 3. In the Back Scattered Electron (BSE) images, a brighter phase is found in the two specimens doped with Bi

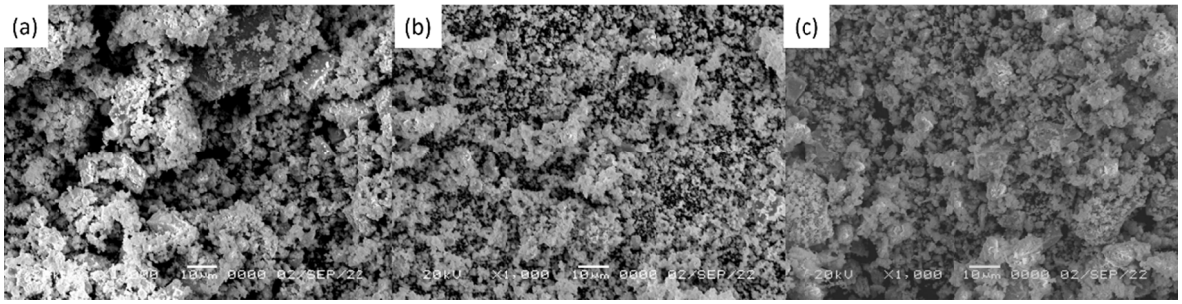

Fig. 2. SEM images of ball-milled powder (a) with Sn and Se, (b) with Bi, Sn, and Se, and (c) with Bi_2O_3, Sn, and Se

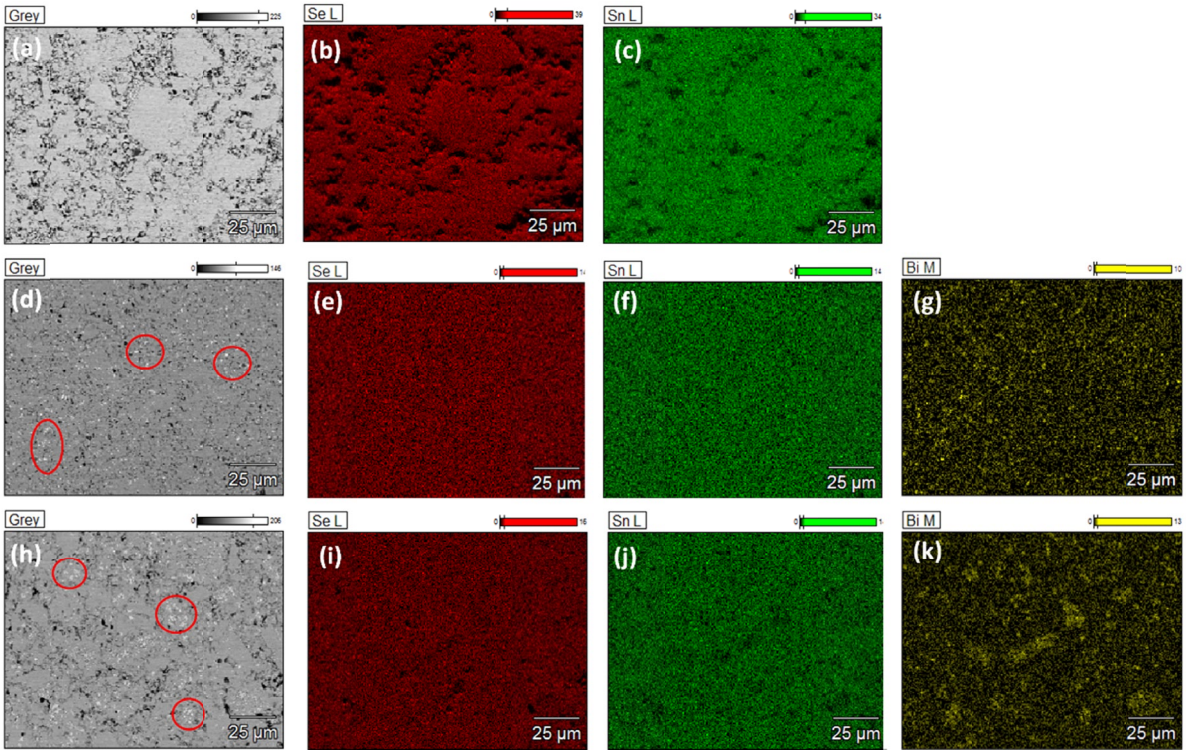

Fig. 3. SEM images and EDS mapping of sintered body: (a-c) SnSe, (d-g) Bi-$Sn_{0.94}Bi_{0.06}Se$, and (h-k) Bi_2O_3-$Sn_{0.94}Bi_{0.06}Se$

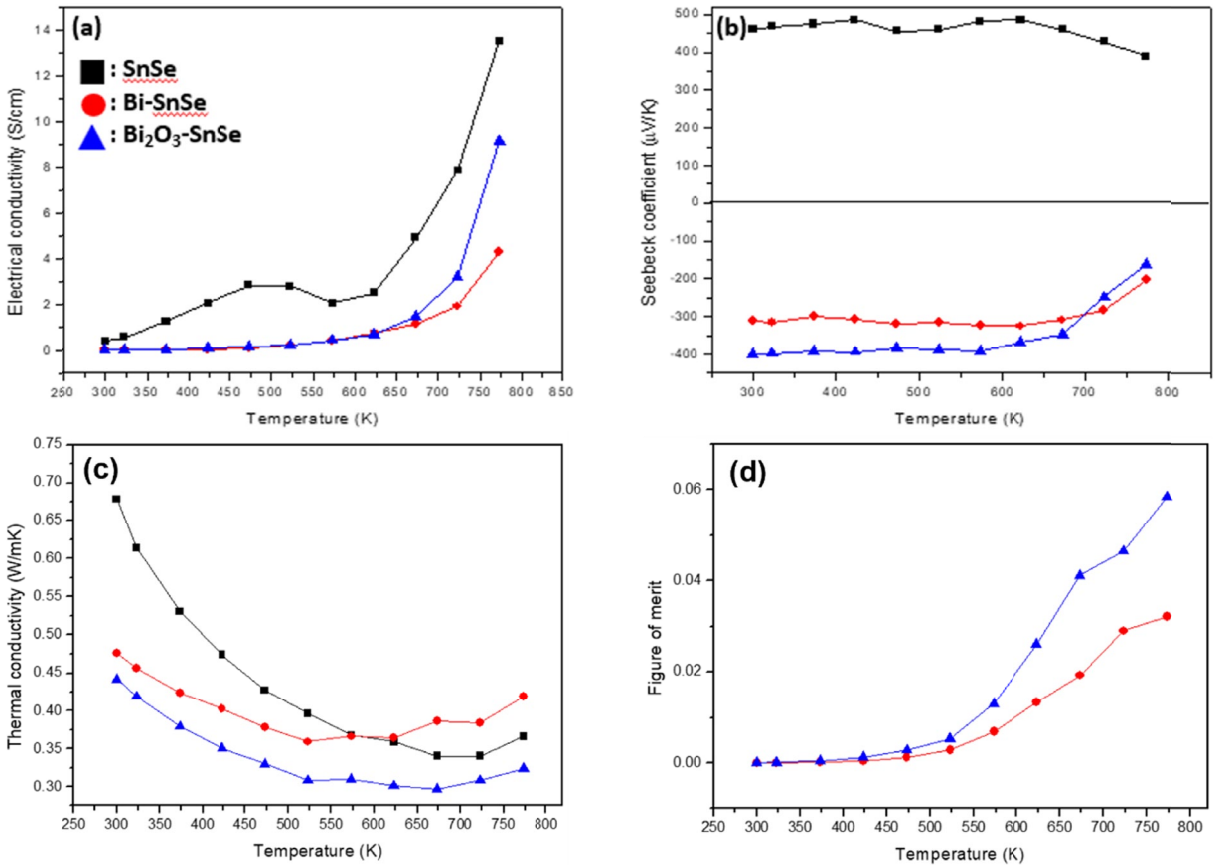

Fig. 4. Temperature-dependent (a) electrical conductivity, (b) Seebeck coefficient, (c) thermal conductivity, and (d) figure of merit of SnSe (indicated by black line), Bi-$Sn_{0.94}Bi_{0.06}Se$ (indicated by red line), and Bi_2O_3-$Sn_{0.94}Bi_{0.06}Se$ (indicated by blue line) measured along the compaction direction

compared to SnSe. This result is due to relatively heavy elements, such as Bi, forming bright images in EDS images. Through the EDS mapping image and XRD pattern, it can be confirmed that other phases, such as Bi_2Se_3, are not precipitated.

Fig. 4 shows the electrical conductivity, Seebeck coefficient, thermal conductivity measured in the direction parallel to the compaction direction, and figure of merit calculated based on the measured values. The relative density of the specimen prepared using Bi was 92.4%, and the relative density of the specimen prepared using Bi_2O_3 was 93.7%. The increase in density is expected to increase the electrical conductivity. In Fig. 4(b), the Seebeck coefficient was positive in the case of SnSe, while the Bi-doped specimens, Bi-$Sn_{0.94}Bi_{0.06}Se$ and Bi_2O_3-$Sn_{0.94}Bi_{0.06}Se$ had negative values. It means that Bi was successfully substituted Sn sites [11,19]. Through this, it can be confirmed that the type has been changed due to Bi doping. In Fig. 4(c), the thermal conductivity can be confirmed. In the process of reducing Bi_2O_3 to Bi, a liquid phase appeared and the orientation of the (400) plane acting as a cleavage plane increased. It led to higher anharmonicity. As a result, the thermal conductivity of Bi_2O_3-$Sn_{0.94}Bi_{0.06}Se$ was the lowest. In Fig. 4(d), the figure of merit can be confirmed. Compared to the case of using pure Bi, a liquid phase appeared through sintering in a hydrogen atmosphere when using Bi_2O_3, where the improvement of the figure of merit was confirmed through the orientation of the (400) plane and the increase in density.

4. Conclusions

In this study, Bi-doped SnSe was prepared by sintering in a hydrogen atmosphere using Bi_2O_3, Sn, and Se as starting powders, while specimens using pure-Bi instead of Bi_2O_3 and pure-SnSe were prepared for the control group. Then their thermoelectric properties were measured. When Bi was used, mechanical alloying proceeded in the milling step, and it was confirmed that Bi was doped through the shifting of the XRD pattern. The refinement of the powder was also observed due to increased brittleness. Bi_2O_3 was reduced to Bi by sintering in a hydrogen atmosphere. In the process, it was observed that the relative density increased and the orientation of the (400) plane increased due to the appearance of the liquid phase. As a result, it was confirmed that the electrical conductivity increased, and the thermal conductivity decreased. When Bi_2O_3 was used, it was confirmed that the figure of merit increased, and the type changed from p-type to n-type.

Acknowledgments

This study was supported by the Research Program funded by SeoulTech (Seoul National University of Science and Technology).

REFERENCES

[1] F. Tohidi, S.G. Holagh, A. Chitsaz, Appl. Therm. Eng. **201**, 117793 (2022).

[2] X.L. Shi, J. Zou , Z.G. Chen, Chem. Rev. **120**, 7399 (2020).

[3] L. Yang, Z.G. Chen, M. Hong, G. Han, J. Zou, ACS Appl. Mater. Interfaces **7**, 23694 (2022).

[4] K.T. Kim, T. Min, D.W. Kim, J. Powder Mater. **23**, 263 (2016).

[5] L. Yang, Z.G. Chen, M. Hong, L. Wang, D. Kong, L. Huang, G. Han, Y. Zou, M. Dargusch, J. Zou, Nano Energy **31**, 105 (2017).

[6] X. Shi, A. Wu, T. Feng, K. Zheng, W. Liu, Q. Sun, M. Hong, S.T. Pantelides, Z.G. Chen, J. Zou, Adv. Energy Mater. **9**, 1803242 (2019).

[7] M.J. Jung, Y.J. Yun, J. Byun, B.J. Choi, J. Powder Mater. **28**, 239 (2021).

[8] Q. Wen, C. Chang, L. Pan, X. Li, T. Yang, H. Guo, Z. Wang, J. Zhang, F. Xu, Z. Zhang, G. Tang, J. Mater. Chem. A. **5**, 13392 (2017).

[9] C. Zhou, Y.K. Lee, Y. Yu, S. Byun, Z.Z. Luo, H. Lee, B. Ge, Y.L. Lee, X. Chen, J.Y. Lee, O.C. Miredin, H. Chang, J. Im, S.P. Cho, M. Wutting, V.P. Dravid, M.G. Kanatzidis, I. Chung, Nat. Mater. **20**, 1378 (2021).

[10] M. Tewolde, G. Fu, D.J. Hwang, L. Zuo, S. Sampath, P. Longtin, J. Therm. Spray Technol. **25**, 431 (2016).

[11] A.T. Duong, V.Q. Nguyen, G. Duvjr, V.T. Duong, S. Kwon, J.Y. Song, J.K. Lee, J.E. Lee, S. Park, T. Min, J. Lee, J. Kim, S. Cho, Nat. Commun. **7**, 13713 (2016).

[12] S. Kundu, S.I. Yi, C. Yu, Appl. Surf. Sci. **459**, 376 (2016).

[13] S. Chandra, A. Banik, K. Biswas, ACS Energy Lett. **3**, 1153 (2018).

[14] X. Li, C. Chen, W. Xue, S. Li, F. Cao, Y. Chen, J. He, J. Sui, X. Liu, Y. Wang, Q. Zhang, Inorg. Chem. **57**, 13800 (2018).

[15] M.R. Pallavolu, S.K. Vishwanath, S. W. Joo, Mater. Lett. **281**, 128714 (2020).

[16] M. Li, Y. Liu, Y. Zhang, Y. Zuo, J. Li, K.H. Lim, D. Cadavid, K.M. Ng, A. Cabot, Dalton Trans. **48**, 3641 (2019).

[17] N.T. Rochman, K. Kawamoto, H. Sueyoshi, Y. Nakamura, T. Nishida, J. Mater. Process. Technol. **89-90**, 367 (1999).

[18] M. Mccormack, H.S. Chen, G.W. Kammilott, S. Jin, J. Electron. Mater. **26**, 954 (1997).

[19] V.Q. Nguyen, T.H. Nguyen, V.T. Duong, J.E. Lee, S.D. Park, J.Y. Song, H.M. Park, A.T. Duong, S. Cho, Nanoscale Res. Lett. **13**, 200 (2018).